


# Study on the Influence of KOH Wet Treatment on Red $\mu$ LEDs

Shuhan Zhang, Qian Fan, Xianfeng Ni, Li Tao  and Xing Gu \*

Institute of Next Generation Semiconductor Materials, Southeast University, Suzhou 215123, China; 220215005@seu.edu.cn (S.Z.); 103200035@seu.edu.cn (Q.F.); 103200036@seu.edu.cn (X.N.); tao@seu.edu.cn (L.T.)  
\* Correspondence: xinggu@seu.edu.cn

**Abstract:** InGaN-based red micro-light-emitting diodes ( $\mu$ LEDs) of different sizes were prepared in this work. The red GaN epilayers were grown on 4-inch sapphire substrates through metal-organic chemical vapor deposition (MOCVD). Etching, sidewall treatment, and p- and n-contact deposition were involved in the fabrication process. Initially, the etching process would cause undesirable damage to the GaN sidewalls, which leads to an increase in leakage current. Hence, we employed KOH wet treatment to rectify the defects on the sidewalls and conducted a comparative and systematic analysis of electrical as well as optical properties. We observed that the  $\mu$ LEDs with a size of 5  $\mu$ m exhibited a substantial leakage current, which was effectively mitigated by the application of KOH wet treatment. In terms of optical performance, the arrays with KOH demonstrated improved light output power (LOP). Additionally, while photoelectric performance exhibited a decline with increased current density, the devices treated with KOH consistently outperformed their counterparts in terms of optoelectronic efficiency. It is noteworthy that the optimized devices displayed enhanced photoelectric characteristics without significantly altering their original peak wavelength and FWHM. Our findings point to the elimination of surface non-radiative recombination by KOH wet treatment, thereby enhancing the performance of small-sized red  $\mu$ LEDs, which has significant potential in realizing full-color micro-displays in near-eye projection applications.

**Keywords:**  $\mu$ LED; GaN; KOH treatment; sidewall damage



**Citation:** Zhang, S.; Fan, Q.; Ni, X.; Tao, L.; Gu, X. Study on the Influence of KOH Wet Treatment on Red  $\mu$ LEDs. *Crystals* **2023**, *13*, 1611. <https://doi.org/10.3390/cryst13121611>

Academic Editor: Julien Brault

Received: 25 October 2023

Revised: 16 November 2023

Accepted: 18 November 2023

Published: 21 November 2023



**Copyright:** © 2023 by the authors. Licensee MDPI, Basel, Switzerland. This article is an open access article distributed under the terms and conditions of the Creative Commons Attribution (CC BY) license (<https://creativecommons.org/licenses/by/4.0/>).

## 1. Introduction

III-nitride semiconductors, owing to their direct bandgap structure, have the capability to span a broad spectral range encompassing deep ultraviolet through near-infrared regions with alloy compositions [1,2]. The remarkable achievement of III-nitride semiconductors lies in the innovation and maturation of highly efficient InGaN-based blue and green light-emitting diodes (LEDs) [3,4], which have undergone commercial production for several years and have found extensive utilization in lighting and display applications [5].

With the continuous advancement of research on LEDs by researchers, up until the present, InGaN-based micro-light-emitting diode ( $\mu$ LED) is considered to be the most promising next-generation display technology, which has greater advantages over liquid crystal display (LCD) and organic LED (OLED) in terms of brightness, resolution, contrast, power consumption, reliability, response speed, and thermal stability [6]. As a result, it is now the ideal solution for numerous applications such as virtual reality (VR) and augmented reality (AR) [7].

At present, most blue and green LEDs employ InGaN materials, while red LEDs utilize AlGaInP. Larger AlGaInP red LEDs are highly efficient, with a wall-plug efficiency (WPE) exceeding 50% under simulation, but their efficiency drops significantly when scaled down to the  $\mu$ LED range due to increased surface recombination and longer carrier diffusion lengths [8]. AlGaInP red LEDs are also sensitive to temperature changes, which can cause efficiency losses due to carrier leakage [9]. Integrating RGB  $\mu$ LEDs leads to mismatched light distribution between InGaN and AlGaInP, resulting in undesirable color shifts at different angles for micro-displays. Therefore, extending the emission wavelength of

InGaN-based LEDs from blue/green to red offers a promising alternative to AlGaInP for micro-displays [10].

However, the development of  $\mu$ LEDs still faces a substantial number of challenges. Among them, the high-quality fabrication and processes of InGaN-based red  $\mu$ LED are essential to achieve homogeneous and integrated full-color displays. In this regard, researchers continually make breakthroughs in various directions. Regarding transfer technologies, Chang et al. proposed the MDSAT method, which combines magnetic and dielectrophoresis (DEP) forces, for the rapid transfer of RGB LEDs onto large-area substrates, surpassing the previous FSA approach, and the transfer efficiency of RGB LEDs reached 99.99% by optimization [11]. In the context of substrate optimization, White et al. presented their findings, demonstrating that red InGaN  $\mu$ LEDs achieved an EQE approaching 1% by employing semi-relaxed InGaN substrates on sapphire [12]. Li et al., leveraging substrate optimization, have developed red  $\mu$ LEDs with an EQE of 4.5% by employing epitaxial tunnel junction (TJ) contact [13]. In devices, Son et al. successfully enhanced the light output power and current density of GaN-based blue  $\mu$ LEDs by employing a  $\mu$ LED array structure. The enhancement rates of the output power were 174%, and in current density, it was enhanced by a factor of 2.1 when compared to that of the reference one [14]. Mei et al. achieved heightened light extraction efficiency in GaN-based  $\mu$ LED devices by a suspended structure, which was 150% higher than that of the normal device [15]. On the other hand, the size reduction tends to have a large impact on device performance. The rise in the body-to-surface area ratio of  $\mu$ LEDs as their size diminishes significantly affects their efficiency and leakage current. This phenomenon is attributed to the sidewall effect, which is induced by the plasma dry etching process, resulting in increased damage density and an elevated density of Shockley–Read–Hall (SRH) non-radiative recombination centers [16]. Therefore, to improve the performance of small-sized red  $\mu$ LEDs, sidewall treatment is crucial in the device fabrication process.

There are currently two main types of treatments available to reduce the sidewall effect. One is the different types of aqueous solutions, which include KOH, tetramethylammonium hydroxide (TMAH), and  $\text{H}_3\text{PO}_4$  [17]. Yang et al. discovered that subjecting GaN-based LEDs to a 20% KOH treatment for 60 min at 100 °C can effectively optimize forward turn-on characteristics and suppress leakage currents [18]. Wong et al. demonstrated that the combination of KOH chemical treatment and ALD sidewall passivation can effectively reduce the SRH non-radiative recombination and surface recombination caused by plasma damage by presenting the peak EQE (22–25% at 5–15  $\text{Acm}^{-2}$ ) of the blue InGaN LEDs (sizes range from 10–100  $\mu\text{m}$ ) [19]. Sun et al. studied that tetramethylammonium hydroxide (TMAH) wet treatment optimized the micro trench at the bottom corner of the mesa sidewall [20]. Mahitosh et al. improved the internal quantum efficiency of the near-band-edge emission peak from 3% to 7% through phosphoric acid [21]. The other type of treatment is conducted by dielectric materials passivation, which includes but is not limited to  $\text{SiO}_2$ ,  $\text{SiNx}$ , and  $\text{Al}_2\text{O}_3$  [17]. Hsu et al. used a hybrid  $\text{SiO}_2$  micro/nanospheres antireflection coating to obtain a lower leakage current and achieve an 18.7% improvement in the light output power [22]. Even for passivation layers of the same material, the use of different processes can have different effects on the performance of the LEDs. Lee et al. conducted an investigation demonstrating that the ALD- $\text{Al}_2\text{O}_3$ /PECVD- $\text{SiO}_2$  passivation layer exhibits superior performance in suppressing sidewall effects compared to the PECVD- $\text{SiO}_2$  layer alone. Furthermore, at lower current densities, the double passivation layer achieves peak external quantum efficiency, surpassing that of the single-layer counterparts [23]. Chevtchenko et al. proved that a reduction of the leakage current can be observed after  $\text{SiNx}$  passivation, and passivation eliminates surface states and surface recombination [24]. Kim et al. applied  $\text{AlN}/\text{Al}_2\text{O}_3$  deposition on p-GaN to acquire LEDs with higher light-emission efficiency and a minimized leakage current [25].

In this research, red InGaN-based  $\mu$ LED arrays with different sizes ( $5\ \mu\text{m} \times 5\ \mu\text{m}$ ,  $10\ \mu\text{m} \times 10\ \mu\text{m}$ ,  $15\ \mu\text{m} \times 15\ \mu\text{m}$ ,  $20\ \mu\text{m} \times 20\ \mu\text{m}$ ) were successfully fabricated, based on which we systematically investigated the effects of treatment with or without KOH on the sidewalls. Characterization of the sidewall morphology and electrical and optical properties of the device were conducted through scanning electron microscopy (SEM), current–voltage curves, and electroluminescence (EL), aiming to assess its performance.

## 2. Materials and Methods

The red LED arrays were fabricated on GaN epi layers, which were grown on a 4-inch sapphire substrate by the metal-organic chemical vapor deposition (MOCVD) method by Suzhou Hanhua Semiconductors Ltd., (Suzhou, China). The epitaxial structure is shown in Figure 1a. The LEDs were grown on 4-inch planar sapphire substrates. The epitaxial growth started with 30 nm low-temperature GaN, which serves as a nucleation layer for subsequent growth. Then, a 1.5  $\mu\text{m}$ -thick un-intentionally doped (UID) GaN layer was grown until its surface coalesced, which was followed by a 2.5  $\mu\text{m}$  n-type GaN contact layer doped with Si to  $5 \times 10^{18}\ \text{cm}^{-3}$ . After the n-type contact layer, a 200 nm InGaN-based strain-release layer and active region (multiple-quantum wells, MQWs) were deposited. On top of the active region, a p-type electron-blocking layer (EBL) as well as a p-type GaN and a p-type contact layer were grown. All the p-type layers were doped with Mg.

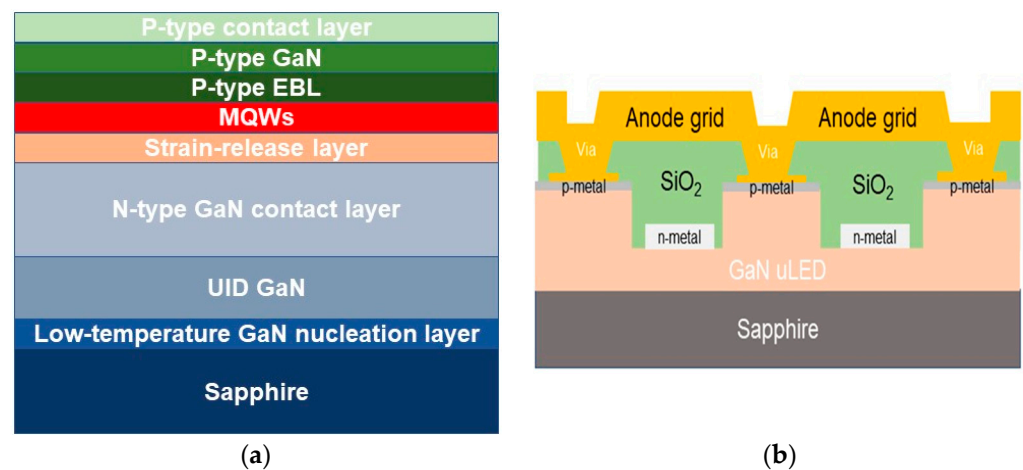


**Figure 1.** (a) Schematic for the epitaxial structure of the LEDs; (b) cross-section structure of the  $\mu$ LED array used in this paper.

After the epitaxial growth, the LED materials were p-type activated by thermal annealing in a furnace. The materials were then characterized by photoluminescence (PL) with a laser wavelength at 405 nm, as well as electroluminescence (EL) with an indium dot directly on the wafer surface. The diameter of the indium dot was around 1.5–2.0 mm. The LED wafers were then fabricated into devices. The device structure ensures that the light is reflected towards the substrate direction during the optical measurement, and the detailed fabrication processes are described below, and the schematic of the device process is depicted in Figure 2.

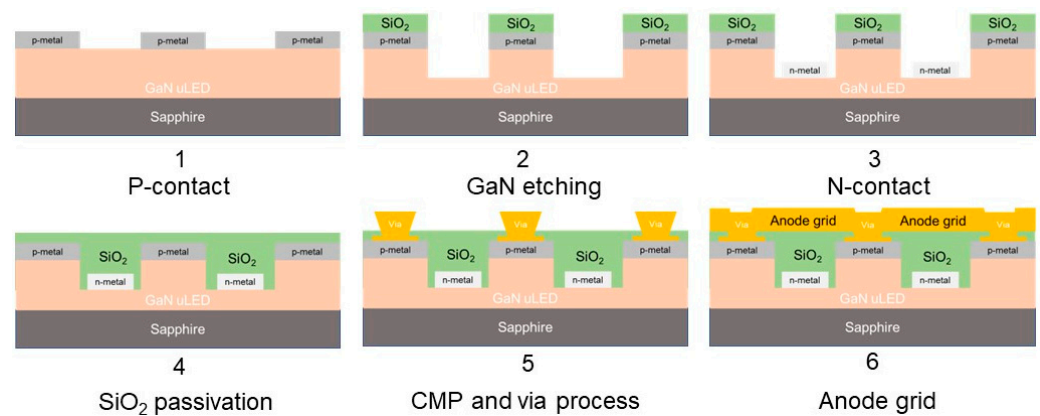


**Figure 2.** Schematic of the device process.

Initially, to remove the contaminations on the surface of the wafers, organic and acid cleaning is performed. Then, a 20 nm thick NiAu layer is deposited on the p-GaN using electron beam evaporation, followed by an annealing process in an oxygen atmosphere at 550 °C for 1 min to facilitate the formation of improved ohmic contacts. For mesa formation, photolithography is employed in conjunction with an 800 nm thick silicon dioxide (SiO<sub>2</sub>) hard mask. The SiO<sub>2</sub> hard mask is grown by plasma-enhanced chemical vapor deposition (PECVD), followed by patterning and etching of SiO<sub>2</sub> using a fluorine-based inductively coupled plasma (ICP) etching technique. LED mesa is formed by a chlorine-based inductively coupled plasma reactive ion etching process reaching the n-GaN layer. Then, sidewall treatment is conducted on selected wafers by soaking them in a KOH solution at 80 °C for 3 min. The SiO<sub>2</sub> hard mask serves to preserve the integrity of the top surface of the device's p-GaN, including the NiAu layer. After that, the n-contacts grid pattern is deposited on the n-GaN surface between LEDs. Subsequently, a 2.5 μm thick SiO<sub>2</sub> passivation layer is deposited, and the wafer surface is planarized by a chemical mechanical polishing (CMP) process, concurrently reducing the thickness of the SiO<sub>2</sub> to 200 nm, followed by a process to open the p-metal of each LED. Following this, an etching process is employed to remove the SiO<sub>2</sub> layer on the n-pad, ensuring that the n-pad is exposed for subsequent electrical and optical measurement purposes. In each array that contains tens of thousands of LEDs, we placed an anode grid consisting of TiAl, which is deposited by sputtering, to shoot the p-contact of all pixels to facilitate the electrical and optical measurement by driving them together. The sizes of the LEDs in the different arrays include 5 × 5 μm, 10 × 10 μm, 15 × 15 μm, and 20 × 20 μm. The cross-section structure of the array is illustrated in Figure 1b.

### 3. Results

In the PL (photoluminescence) measurement conducted at room temperature with a laser wavelength of 405 nm, we obtained photoluminescence images of the entire epi wafer surface. As is shown in Figure 3, these images reveal the distribution of W<sub>p</sub> (peak wavelength) and FWHM (full width at half maximum) in different regions, thereby providing spatial distribution information about the material properties within the epi wafer. In the figure, it is observed that the W<sub>p</sub> of both epi wafers is centered at 673 nm. Furthermore, the FWHM of the epi wafer intended for the KOH wet treatment is concentrated at 87 nm, while the FWHM for the other wafer is centered at 90 nm. These two epi wafers exhibit similar characteristics. By analyzing the PL mapping figure, we can observe that these two epi wafers exhibit good uniformity in terms of W<sub>p</sub> and FWHM, which meets our requirements for utilizing them in subsequent processes.

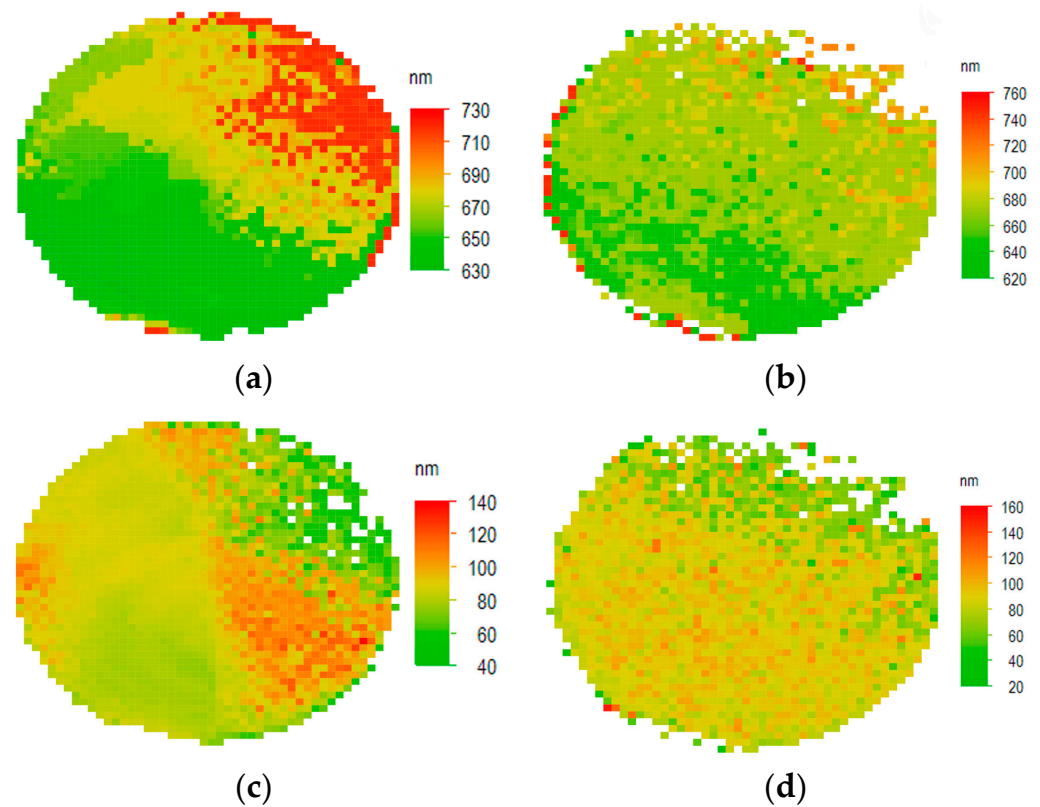
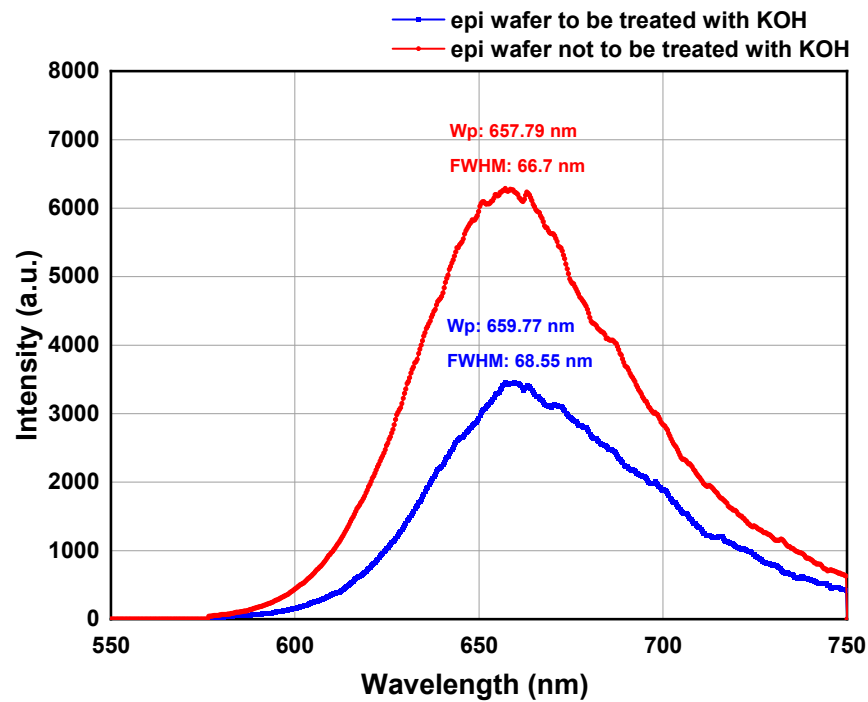


**Figure 3.** (a) PL mapping of Wp on the epi wafer to be treated with KOH at room temperature with a laser wavelength of 405 nm; (b) PL mapping of Wp on the epi wafer not to be treated with KOH at room temperature with a laser wavelength of 405 nm; (c) PL mapping of FWHM on the epi wafer to be treated with KOH at room temperature with a laser wavelength of 405 nm; (d) PL mapping of FWHM on the epi wafer not to be treated with KOH at room temperature with a laser wavelength of 405 nm.

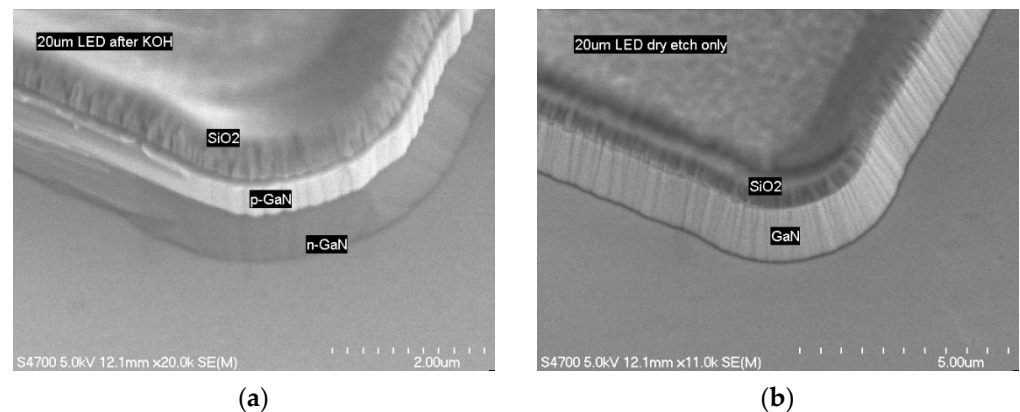
Figure 4 presents the EL (electroluminescence) spectral data of the epi wafers obtained at an injection current of 109 mA. The blue line represents the epi wafer intended for subsequent KOH sidewall treatment, while the red line represents the epi wafer that will not undergo KOH wet treatment. In the figure, we observe that the properties of these two epi wafers are similar, with comparable values for Wp and FWHM, showing minimal differences. This phenomenon is attributed to the identical epitaxial conditions employed for both epi wafers. Specifically, the epitaxial structure, composition of each layer, layer thickness, doping conditions, and other relevant parameters were maintained uniformly across both epi wafers. Therefore, these two epi wafers can be further processed, effectively controlling variables for subsequent comparisons of various properties.

Figure 5a,b show scanning electron microscope (SEM) images for a comparison between the LED mesa with KOH wet treatment and the one without. In this context, we have selected a mesa with a size of 20  $\mu\text{m}$  for our illustrative example. From the figure, it is obvious that after the dry etching process, the GaN sidewalls exhibit a significantly roughened texture. In contrast, after wet KOH etching, the GaN sidewalls appear considerably smoother, indicating an effective removal of sidewall GaN material. This treatment serves to reduce the density of the leakage path on the sidewalls.





**Figure 4.** Wp and FWHM of epi wafers under the injected current of 109 mA, utilizing indium dots with a diameter of 1.5 mm as the *p*-contact.



**Figure 5.** (a) SEM images of a mesa with a size of 20  $\mu\text{m}$  with KOH wet treatment; (b) SEM images of a mesa with a size of 20  $\mu\text{m}$  without KOH treatment.

Figure 6 shows the current–voltage (*I*–*V*) curves of array devices of different sizes with or without KOH wet etching. Figure 6a displays the *I*–*V* curves for an array device comprising 10,000 pixels. In this array, the individual LED size is 20  $\mu\text{m}$ . The blue line represents the group in which KOH sidewall etching was performed, while the red line corresponds to the control group, which did not undergo KOH etching. In terms of leakage current, we find that at  $-5\text{V}$ , the leakage current density without KOH is  $0.2965\text{ A/cm}^2$  and the leakage current density with KOH wet treatment is  $0.0131\text{ A/cm}^2$ , which is obviously lower. Similar trends are observed on all arrays in different sizes:  $0.007\text{ A/cm}^2$ ,  $0.0012\text{ A/cm}^2$ , and  $0.0057\text{ A/cm}^2$  for 15  $\mu\text{m}$ , 10  $\mu\text{m}$ , and 5  $\mu\text{m}$  size pixels with KOH treatment and  $0.0144\text{ A/cm}^2$ ,  $0.0057\text{ A/cm}^2$ , and  $0.6652\text{ A/cm}^2$  for the same size pixels without treatment. Through a comparative analysis of data, it is observed that the leakage current has decreased by a minimum factor of 2.06 and by a maximum of two orders of magnitude. Both scenarios exhibit a noticeable inhibitory effect on the leakage current, which indicates that KOH sidewall wet etching can eliminate the defects caused during dry etching well, allowing the leakage current to be reduced to an ideal state.

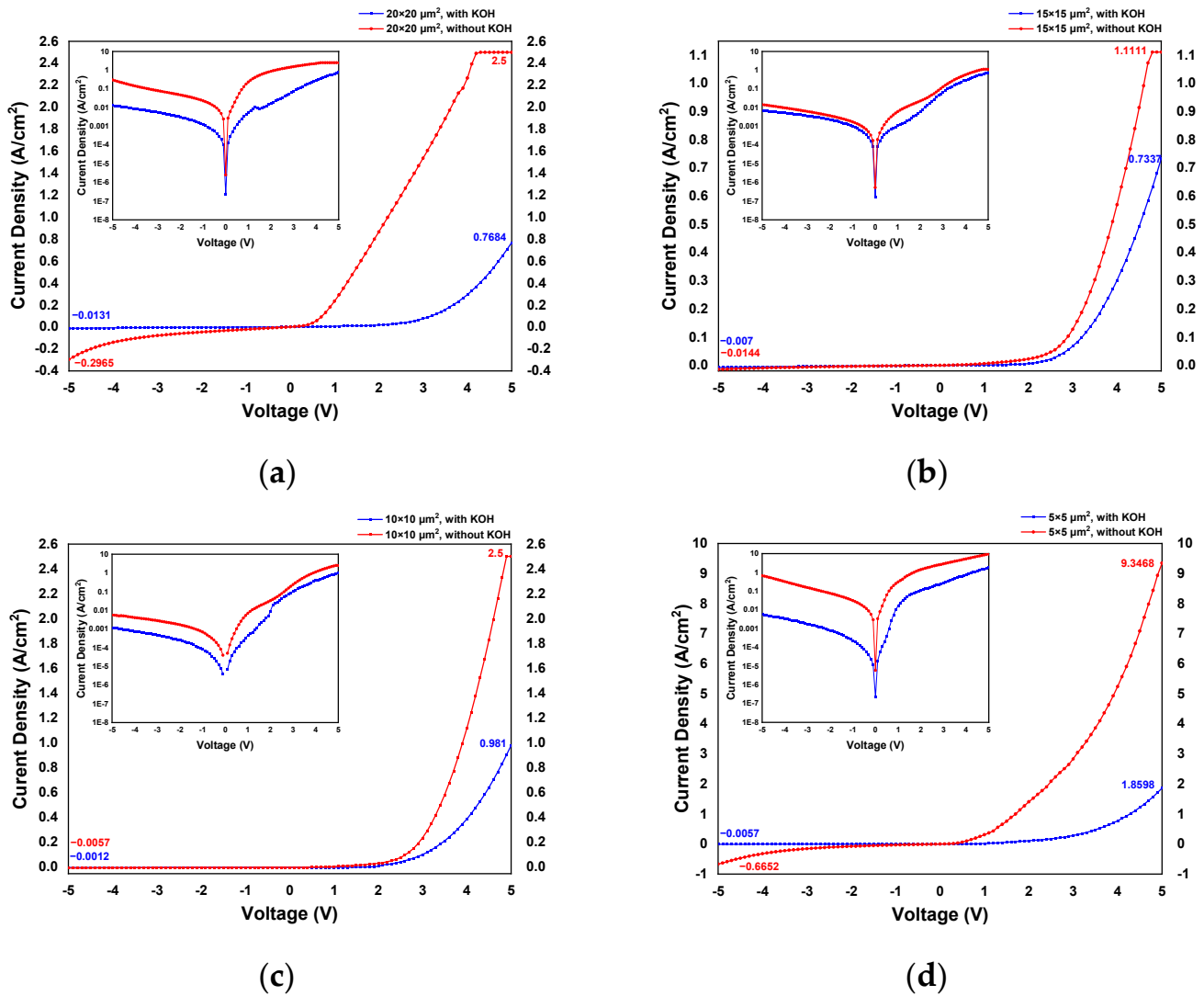


**Figure 6.** I–V characteristic for arrays with different sizes. (a) I–V characteristic for arrays with a size of 20  $\mu\text{m}$ ; (b) I–V characteristic for arrays with a size of 15  $\mu\text{m}$ ; (c) I–V characteristic for arrays with a size of 10  $\mu\text{m}$ ; (d) I–V characteristic for arrays with a size of 5  $\mu\text{m}$ .

In the presented data, the effectiveness of KOH wet etching in mitigating the leakage current is consistent through a wide range of device sizes. Furthermore, there exists a substantial correlation between the density of leakage current and device size. Specifically, for smaller-sized LEDs, as their dimensions decrease, the body-to-surface area ratio steadily increases. Consequently, this heightened ratio leads to an augmentation in surface states within the LED structure. Surface states, in this context, refer to electronic states positioned within or near the energy bandgap or band edges, which are capable of capturing and releasing charge carriers, such as electrons. In the case of smaller-sized LEDs, the relatively larger surface area compared to volume facilitates a more pronounced influence of these surface states on electron dynamics. This influence results in an increase in leakage current density. Remarkably, at a dimension of 5  $\mu\text{m}$ , the LED array exhibits the highest leakage current density. However, KOH wet treatment to the sidewalls significantly ameliorates this issue, elevating the leakage current density to a level commensurate with arrays of other sizes. This improvement arises primarily from the ability of KOH wet etching to optimize the removal of damage, defects, and impurities introduced during dry etching processes. This optimization reduces lattice imperfections, refines electric field distribution, diminishes electron scattering in proximity to sidewalls, and minimizes leakage pathways. KOH wet

etching serves to lower surface state density, further reducing the impact of surface states on electron behavior, thus contributing to the reduction of the leakage current.

Figure 7 shows the EL spectra obtained at the injection current of 200 mA for different-sized arrays, where Wp and FWHM can be obtained for cases with (Figure 7a) and without (Figure 7b) KOH treatment. From the figures, we see that the Wp consistently exceeds 632 nm, with FWHM ranging around 60 nm. Comparing the epi wafer data in Figure 4, we observe that after device processing, Wp and FWHM have not undergone significant changes. This indicates that our device processing has not adversely affected the material's inherent performance. Notably, neither Wp nor FWHM exhibits any significant trends resulting from KOH wet treatment. Furthermore, both pictures show that at the same injection current, a reduction in size corresponds to a decrease in Wp. The underlying cause of this phenomenon is the blue shift at a higher injection current density.

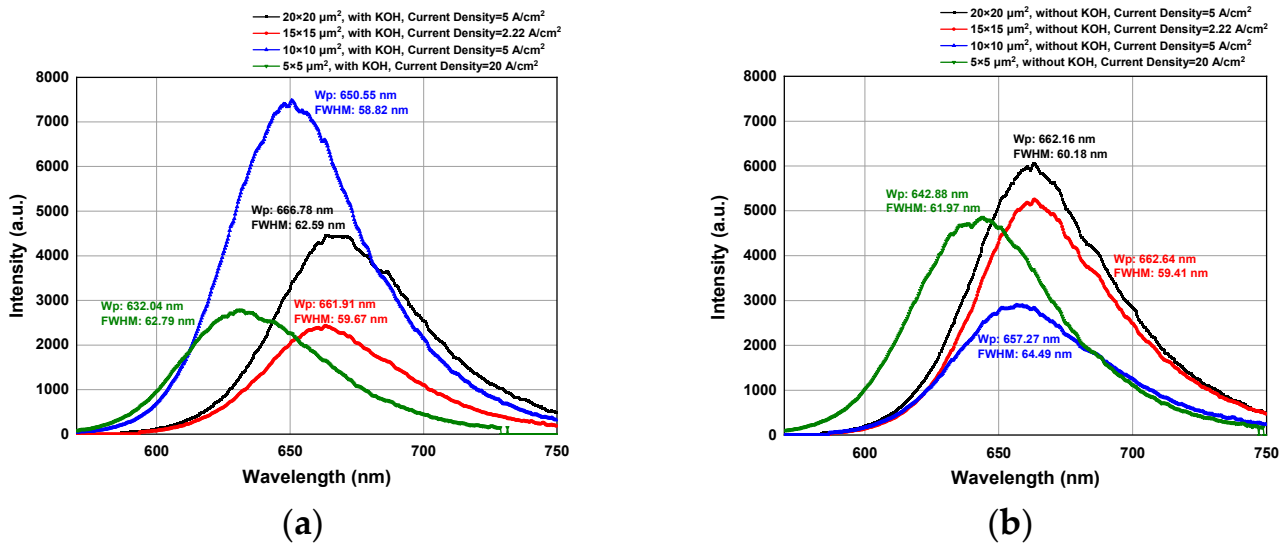


**Figure 7.** Wp and FWHM of arrays with different sizes and treatment under the injected current of 200 mA. (a) Wp and FWHM of arrays treated with KOH; (b) Wp and FWHM of arrays not treated with KOH.

To further investigate the blue shift effect, we also tested the relationship between Wp and the current for four different sizes, as shown in Figure 8, where the blue and red curve represents treatment with and without KOH, respectively. From these data, it can be seen that under an increased current, arrays of varying sizes and processing methods all exhibit a blue shift phenomenon. The change of Wp from an injection current of 100 mA to 300 mA (approximately from  $1.11 \text{ A}/\text{cm}^2$  to  $30 \text{ A}/\text{cm}^2$ ) is usually within 3–8 nm, regardless of the size of the pixel. Furthermore, there appears to be no significant correlation between the blue shift in Wp and the application of KOH wet etching. We believe it is mostly dependent on the red LED epitaxy structures and growth process rather than on the device fabrication process. Usually, the blue shift in InGaN-based LEDs is the result of the screening in the quantum-confined Stark effect (QCSE) and band-filling effects [26], which is especially obvious in high In-concentration for long wavelength MQW structures. The LED wafer we used for this study contains complicated stress relief structures beneath the active region. Compared with other commercially available red GaN epi, our structure shows much elevated performance in terms of blue shift reduction.



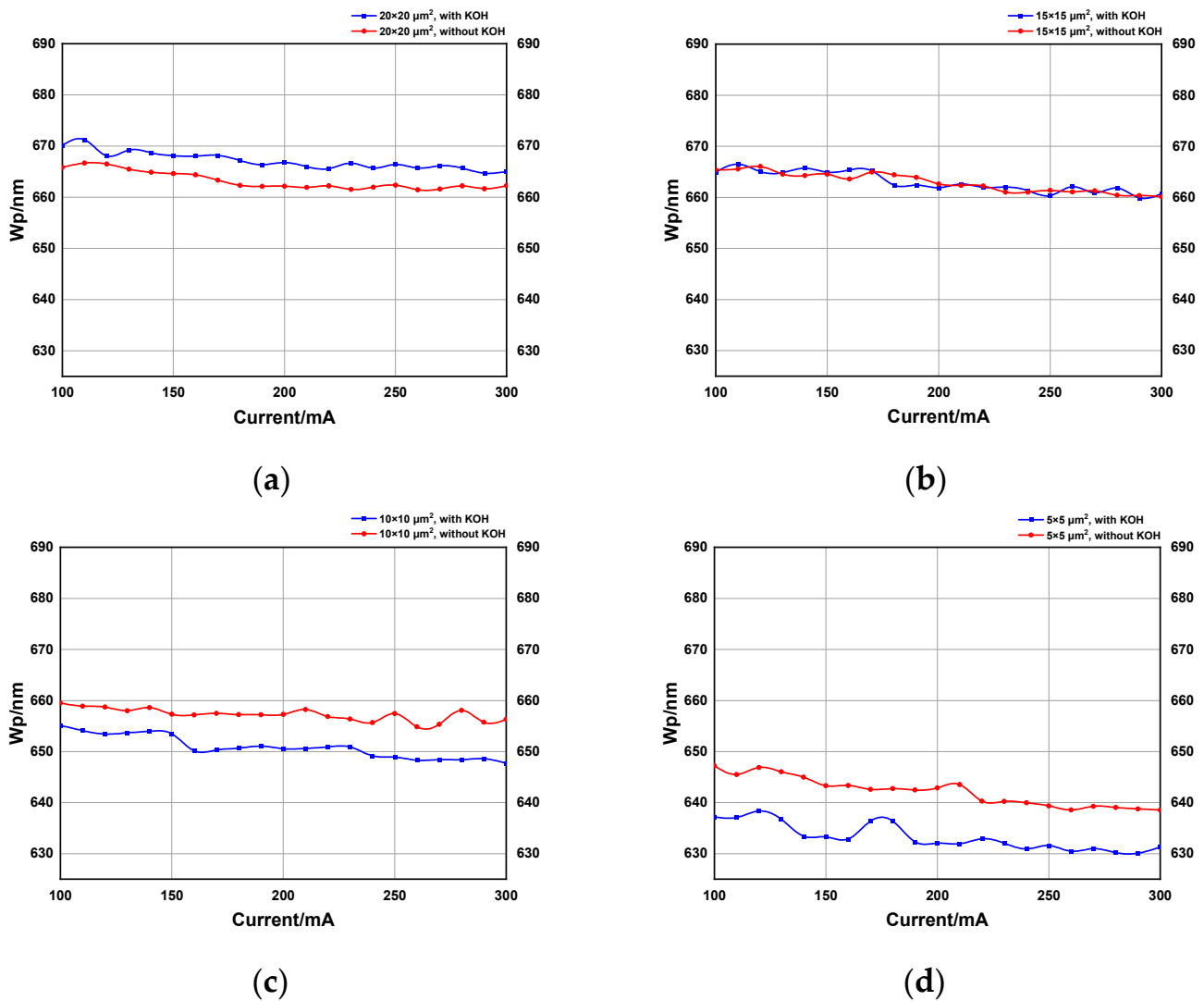


**Figure 8.** Wp under different driving currents for arrays with different sizes. (a) Wp under different driving currents for arrays with a size of 20  $\mu\text{m}$ ; (b) Wp under different driving currents for arrays with a size of 15  $\mu\text{m}$ ; (c) Wp under different driving currents for arrays with a size of 10  $\mu\text{m}$ ; (d) Wp under different driving currents for arrays with a size of 5  $\mu\text{m}$ .

Figure 9 provides a comparison of the light output power (LOP) of  $\mu\text{LEDs}$  between arrays with different sizes. In each figure, the blue curve represents the trends in LOP for arrays subjected to KOH wet treatment, while the red curve signifies the trends for arrays without KOH. The figures clearly indicate that as the injection current density increases, the LOP of LEDs with different sizes and processing methods exhibits a consistent and monotonic increase. Furthermore, it is evident from the figures that arrays with KOH display higher LOP compared to those without KOH treatment. We propose that this occurrence is due to the reduced leakage current in arrays with KOH and allows a more efficient conversion from electrical power into optical power. This suggests that the KOH wet treatment, by modifying the sidewalls and reducing non-radiative recombination centers, can effectively enhance the optical performance of  $\mu\text{LEDs}$ .

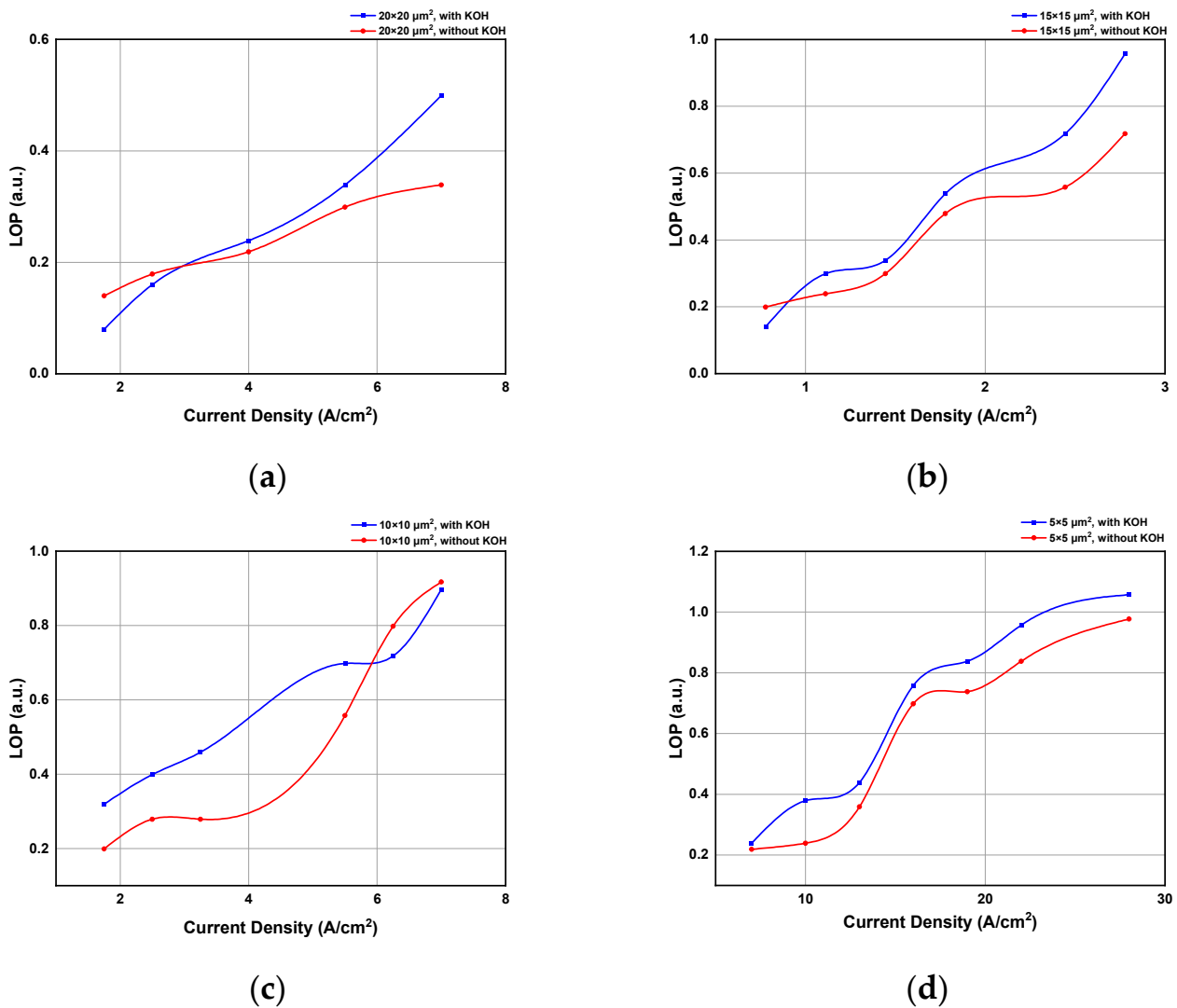


**Figure 9.** LOP under different driving currents for arrays with different sizes. (a) LOP under different driving currents for arrays with a size of 20  $\mu\text{m}$ ; (b) LOP under different driving currents for arrays with a size of 15  $\mu\text{m}$ ; (c) LOP under different driving currents for arrays with a size of 10  $\mu\text{m}$ ; (d) LOP under different driving currents for arrays with a size of 5  $\mu\text{m}$ .

In order to verify the EL (electroluminescent) efficiency of the device, we measured the efficiency droop for a 10  $\mu\text{m}$  size  $\mu\text{LED}$  array, and the result is shown in Figure 10. It is important to note that the efficiency is presented as a relative value rather than an absolute one, so it is only meaningful in comparing the efficiency between devices in the same geometry. The blue curves represent trends observed in arrays with KOH wet treatment, while the red curves represent trends in arrays without KOH. This figure obviously demonstrates that, as the current density steadily increases, electroluminescent efficiency gradually decreases. We attribute this phenomenon to the increased rate of non-radiative recombination as the injected carrier density goes higher. This is well-known as the efficiency droop effects observed in all InGaN-based LEDs. It is noteworthy that, following KOH wet treatment, although the LED efficiency surpasses that of the ones without KOH treatment, it also drops faster as the current goes higher. This observation suggests that the cause for the droop is less likely to originate from the surface defect but is more related to material defects in the epi structure.

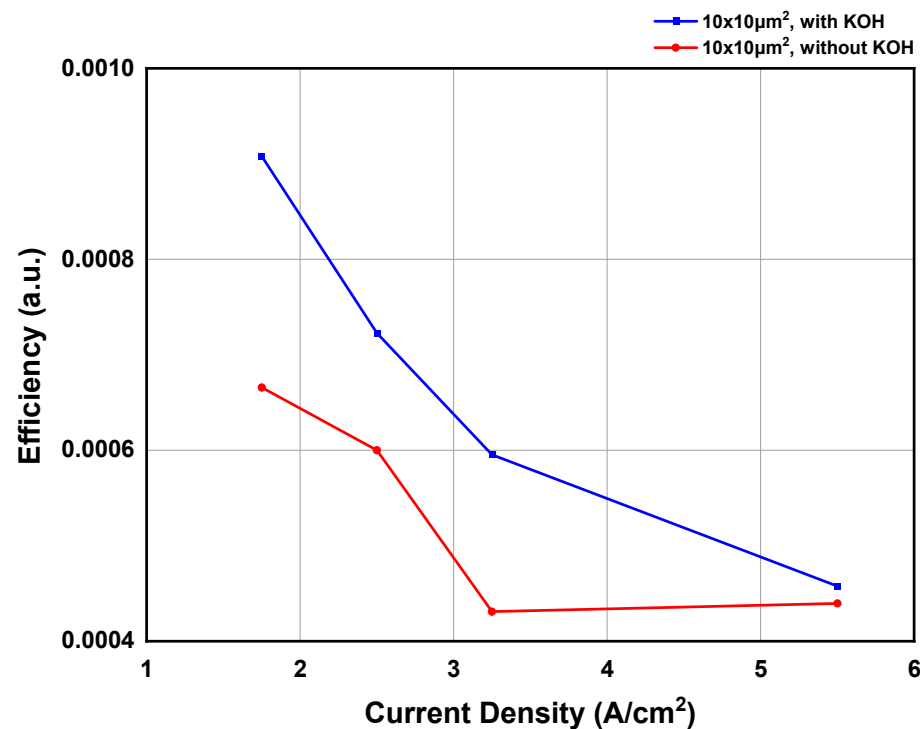


Figure 10. Efficiency under different driving currents for arrays the size of 10  $\mu\text{m}$ .

#### 4. Conclusions

In our study, we have successfully fabricated red  $\mu\text{LED}$  arrays with sizes ranging from 5  $\mu\text{m}$  to 20  $\mu\text{m}$  and demonstrated that their optoelectronic performance can be enhanced by KOH wet treatment on pixel sidewalls. The KOH wet treatment manifests obvious morphology changes on sidewalls and significant reductions in leakage current. Sidewall etching with KOH is an irreversible process, where the severed leakage pathways cannot be recovered, effectively impeding the generation of leakage current. The extent of improvement is more pronounced for smaller-sized  $\mu\text{LED}$ s, particularly those with a size of 5  $\mu\text{m}$ .

Regarding optical performance,  $W_p$  and FWHM remained largely unaffected by different device sizes and treatments. Meanwhile, LOP exhibited a monotonic increase with a rising current density. The minimum  $W_p$  blue shift observed on the different-size arrays indicates superb epi-quality from the MOCVD growth of epi structure. However, in terms of electroluminescent efficiency, although the efficiency for the treated array is better than the non-treated counterpart, it also drops faster. This suggests that the KOH wet treatment to the  $\mu\text{LED}$  pixel sidewalls has great potential to be applied in the device fabrication process to suppress surface non-radiative recombination and improve the optical performance. The efficiency droop is more likely to be related to epi defects, which need extra optimization. In this study, the successful fabrication of small-sized red  $\mu\text{LED}$ s and the optimization by KOH wet treatment of the processes provide support and impetus for expanding their application areas and enhancing display and lighting qualities.

**Author Contributions:** Conceptualization, S.Z. and X.G.; Data curation, S.Z. and X.G.; Funding acquisition, X.G.; Investigation, Q.F., X.N. and L.T.; Resources, Q.F., X.N. and L.T.; Visualization, S.Z.; Writing—original draft, S.Z.; Writing—review and editing, X.G. All authors have read and agreed to the published version of the manuscript.

**Funding:** This research was funded by the National Nature Science Foundation of China, grant numbers 62074033 and 92164102.

**Data Availability Statement:** Data are contained within the article.

**Acknowledgments:** The authors would like to thank Maxwell QH from Dulwich College Suzhou for his contribution to the English language and style in this work.

**Conflicts of Interest:** The authors declare no conflict of interest.

## References

1. Kneissl, M.; Seong, T.Y.; Han, J.; Amano, H. The emergence and prospects of deep-ultraviolet light-emitting diode technologies. *Nat. Photonics* **2019**, *13*, 233–244. [[CrossRef](#)]
2. Damilano, B.; Gil, B. Yellow-red emission from (Ga, In)N heterostructures. *J. Phys. D Appl. Phys.* **2015**, *48*, 403001. [[CrossRef](#)]
3. Nakamura, S. Background Story of the Invention of Efficient InGaN Blue-Light-Emitting Diodes (Nobel Lecture). *Angew. Chem. Int. Ed.* **2015**, *54*, 7770–7788. [[CrossRef](#)] [[PubMed](#)]
4. Wu, Y.; Ma, J.; Su, P.; Zhang, L.; Xia, B. Full-Color Realization of Micro-LED Displays. *Nanomaterials* **2020**, *10*, 2482. [[CrossRef](#)]
5. Wu, T.; Sher, C.-W.; Lin, Y.; Lee, C.-F.; Liang, S.; Lu, Y.; Huang Chen, S.-W.; Guo, W.; Kuo, H.-C.; Chen, Z. Mini-LED and Micro-LED: Promising Candidates for the Next Generation Display Technology. *Appl. Sci.* **2018**, *8*, 1557. [[CrossRef](#)]
6. Zhou, X.; Tian, P.; Sher, C.W.; Wu, J.; Liu, H.; Liu, R.; Kuo, H.C. Growth, transfer printing and colour conversion techniques towards full-colour micro-LED display. *Prog. Quantum Electron.* **2020**, *71*, 100263. [[CrossRef](#)]
7. Pan, Z.-J.; Chen, Z.-Z.; Jiao, F.; Zhan, J.-L.; Chen, Y.-Y.; Chen, Y.-F.; Nie, J.-X.; Zhao, T.-Y.; Deng, C.-H.; Kang, X.-N.; et al. A review of key technologies for epitaxy and chip process of micro light-emitting diodes in display application. *Acta Phys. Sin.* **2020**, *69*, 198501. [[CrossRef](#)]
8. Bulashevich, K.A.; Karpov, S.Y. Impact of surface recombination on efficiency of III-nitride light-emitting diodes. *Phys. Status Solidi-Rapid Res. Lett.* **2016**, *10*, 480–484. [[CrossRef](#)]
9. Oh, C.H.; Shim, J.I.; Shin, D.S. Current- and temperature-dependent efficiency droops in InGaN-based blue and AlGaInP-based red light-emitting diodes. *Jpn. J. Appl. Phys.* **2019**, *58*, SCCC08. [[CrossRef](#)]
10. Zhuang, Z.; Iida, D.; Ohkawa, K. InGaN-based red light-emitting diodes: From traditional to micro-LEDs. *Jpn. J. Appl. Phys.* **2022**, *61*, SA0809. [[CrossRef](#)]
11. Chang, W.; Kim, J.; Kim, M.; Lee, M.W.; Lim, C.H.; Kim, G.; Hwang, S.; Chang, J.; Min, Y.H.; Jeon, K.; et al. Concurrent self-assembly of RGB microLEDs for next-generation displays. *Nature* **2023**, *617*, 287–291. [[CrossRef](#)] [[PubMed](#)]
12. White, R.C.; Li, H.; Houry, M.; Lynsky, C.; Iza, M.; Keller, S.; Sotta, D.; Nakamura, S.; DenBaars, S.P. InGaN-Based microLED Devices Approaching 1% EQE with Red 609 nm Electroluminescence on Semi-Relaxed Substrates. *Crystals* **2021**, *11*, 1364. [[CrossRef](#)]
13. Li, P.; Li, H.; Zhang, H.; Yang, Y.; Wong, M.S.; Lynsky, C.; Iza, M.; Gordon, M.J.; Speck, J.S.; Nakamura, S.; et al. Red InGaN micro-light-emitting diodes (>620 nm) with a peak external quantum efficiency of 4.5% using an epitaxial tunnel junction contact. *Appl. Phys. Lett.* **2022**, *120*, 121102. [[CrossRef](#)]
14. Son, K.R.; Lee, B.R.; Kim, T.G. Improved optical and electrical properties of GaN-based micro light-emitting diode arrays. *Curr. Appl. Phys.* **2018**, *18*, S8–S13. [[CrossRef](#)]
15. Mei, Y.; Xie, M.; Yang, T.; Hou, X.; Ou, W.; Long, H.; Ying, L.; Liu, Y.; Weng, G.; Chen, S.; et al. Improvement of the Emission Intensity of GaN-Based Micro-Light Emitting Diodes by a Suspended Structure. *ACS Photonics* **2022**, *9*, 3967–3973. [[CrossRef](#)]
16. Olivier, F.; Daami, A.; Licitra, C.; Templier, F. Shockley-Read-Hall and Auger non-radiative recombination in GaN based LEDs: A size effect study. *Appl. Phys. Lett.* **2017**, *111*, 022104. [[CrossRef](#)]
17. Seong, T.Y.; Amano, H. Surface passivation of light emitting diodes: From nano-size to conventional mesa-etched devices. *Surf. Interfaces* **2020**, *21*, 100765. [[CrossRef](#)]
18. Yang, Y.; Cao, X.A. Removing plasma-induced sidewall damage in GaN-based light-emitting diodes by annealing and wet chemical treatments. *J. Vac. Sci. Technol. B* **2009**, *27*, 2337–2341. [[CrossRef](#)]
19. Wong, M.S.; Lee, C.; Myers, D.J.; Hwang, D.; Kearns, J.A.; Li, T.; Speck, J.S.; Nakamura, S.; DenBaars, S.P. Size-independent peak efficiency of III-nitride micro-light-emitting-diodes using chemical treatment and sidewall passivation. *Appl. Phys. Express* **2019**, *12*, 097004. [[CrossRef](#)]
20. Sun, Y.; Kang, X.; Zheng, Y.; Wei, K.; Li, P.; Wang, W.; Liu, X.; Zhang, G. Optimization of Mesa Etch for a Quasi-Vertical GaN Schottky Barrier Diode (SBD) by Inductively Coupled Plasma (ICP) and Device Characteristics. *Nanomaterials* **2020**, *10*, 657. [[CrossRef](#)]
21. Biswas, M.; Chavan, V.; Zhao, S.; Mi, Z.; Chakrabarti, S. Passivation of Surface States of AlGaIn Nanowires Using H<sub>3</sub>PO<sub>4</sub> Treatment to Enhance the Performance of UV-LEDs and Photoanodes. *ACS Appl. Nano Mater.* **2018**, *1*, 1968–1975. [[CrossRef](#)]
22. Hsu, C.-H.; Chan, Y.-C.; Chen, W.-C.; Chang, C.-H.; Liou, J.-K.; Cheng, S.-Y.; Guo, D.-F.; Liu, W.-C. Study of GaN-Based LEDs with Hybrid SiO<sub>2</sub> Microsphere/Nanosphere AntiReflection Coating as a Passivation Layer by a Rapid Convection Deposition. *IEEE Trans. Electron Devices* **2017**, *64*, 1134–1139. [[CrossRef](#)]
23. Lee, D.H.; Lee, J.H.; Park, J.S.; Seong, T.Y.; Amano, H. Improving the Leakage Characteristics and Efficiency of GaN-based Micro-Light-Emitting Diode with Optimized Passivation. *ECS J. Solid State Sci. Technol.* **2020**, *9*, 055001. [[CrossRef](#)]
24. Chevtchenko, S.A.; Reshchikov, M.A.; Fan, Q.; Ni, X.; Moon, Y.T.; Baski, A.A.; Morkoç, H. Study of SiN<sub>x</sub> and SiO<sub>2</sub> passivation of GaN surfaces. *J. Appl. Phys.* **2007**, *101*, 113709. [[CrossRef](#)]

25. Kim, K.; Hua, M.; Liu, D.; Kim, J.; Chen, K.J.; Ma, Z. Efficiency enhancement of InGaN/GaN blue light-emitting diodes with top surface deposition of AlN/Al<sub>2</sub>O<sub>3</sub>. *Nano Energy* **2018**, *43*, 259–269. [[CrossRef](#)]
26. Horng, R.H.; Ye, C.X.; Chen, P.W.; Iida, D.; Ohkawa, K.; Wu, Y.R.; Wu, D.S. Study on the effect of size on InGaN red micro-LEDs. *Sci. Rep.* **2022**, *12*, 1324. [[CrossRef](#)] [[PubMed](#)]

**Disclaimer/Publisher's Note:** The statements, opinions and data contained in all publications are solely those of the individual author(s) and contributor(s) and not of MDPI and/or the editor(s). MDPI and/or the editor(s) disclaim responsibility for any injury to people or property resulting from any ideas, methods, instructions or products referred to in the content.